ORIGINAL ARTICLE

Theodoros Marinopoulos · Lorenzo Zani · Simin Li ·
Vadim V. Silberschmidt

Modelling indentation of human lower-limb soft tissue: simulation parameters and their effects

Abstract Modern developments of biomedical applications demand a better understanding of mechanical behaviour of soft biological tissues. As human soft tissues demonstrate a significant structural and functional diversity, characterisation of their mechanical behaviour still remains a challenge. Limitations related with implementation of mechanical experiments on human participants lead to a use of finite-element models for analysis of mechanical responses of soft tissues to different loads. This study focuses on parameters of numerical simulation considered for modelling of indentation of a human lower limb. Assessment of the effect of boundary conditions on the model size shows that at a ratio of its length to the tissue's thickness of 1.7 for the 3D model this effect vanishes. The numerical results obtained with models employing various sets of mechanical parameters of the first-order Ogden scheme were compared with original experimental data. Furthermore, high sensitivity of the resulting reaction forces to the indenting direction is demonstrated for cases of both linear and angular misalignments of the indenter. Finally, the effect of changes in material parameters and their domain on their contribution to the reaction forces is discussed with the aim to improve our understanding of mechanical behaviour of soft tissues based on numerical methods. The undertaken research with its results on minimal requirements for finite-element models of indentation of soft tissues can support inverse analysis of their mechanical properties and underpin orthopaedic and medical procedures.

1 Introduction

Soft biological tissues are ensembles of cells of various types and their extracellular matrixes that together have a specific functionality. Biological tissues are among the most complex materials in terms of structural heterogeneity. This complicates the characterisation of their mechanical behaviour that depends strongly on the morphological features and mechanical behaviours of the underlying tissues and cell types. A human soft tissue consists of skin, adipose (fat), muscle, veins, each with its own substructure. The result of this complexity is an anisotropic mechanical response [1] varying throughout the tissue with the local morphology. Soft tissues are known to exhibit highly nonlinear [2] and time-dependent behaviours [3]. Due to high water concentration, soft tissues can be considered incompressible. Typically, soft tissues are characterised by their J-shaped stress-strain curves [3] with stress remaining (mostly) proportional to strain at initial small deformation, followed by a steep increase after reaching a certain deformation limit.

Previous studies into mechanics of soft tissues tried to obtain these curves experimentally and characterise the soft tissue both in vivo [4] and in vitro [5]. Since there is no standard sample-preparation protocol for such

Communicated by Andreas Öchsner.

T. Marinopoulos · L. Zani · S. Li · V. V. Silberschmidt (✉)
Loughborough University, Loughborough, Leicestershire, UK
E-mail: V.Silberschmidt@lboro.ac.uk

Table 1 Strain-energy functions of hyperelastic models [19]

Neo-Hookean	$W = C_1(I_1 - 3)$	(1)
Ogden	$W = \sum_{p=1}^{N} \frac{\mu_p}{\alpha_p} \left(\lambda_1^{\alpha_p} + \lambda_2^{\alpha_p} + \lambda_3^{\alpha_p} - 3 \right)$	(2)
Mooney–Rivlin	$W = C_{10} \left(I_1^* - 3 \right) + C_{01}(I_2^* - 3)$	(3)
Polynomial	$W = \sum_{i,j=0}^{n} C_{i,j} (I_1 - 3)^i (I_2 - 3)^j$	(4)
James–Green–Simpson	$W = C_{10}(I_1 - 3) + C_{01}(I_2 - 3) + C_{11}(I_1 - 3)(I_2 - 3) + C_{20}(I_1 - 3)^2 + C_{30}(I_1 - 3)^2$	(5)
Yeoh	$W = \sum_{i=1}^{n} C_i (I_1 - 3)^i$	(6)
Arruda-Boyce	$W = Nk_B\theta\sqrt{n} \left[\beta\lambda_{\text{chain}} - \sqrt{n} \ln \left(\frac{\sin h\beta}{\beta} \right) \right]$	(7)

λ_i represent the stretches in the principal directions; $J = \lambda_1\lambda_2\lambda_3$; I_i are the invariants of the Cauchy–Green deformation tensor; n is the number of chain segments, k_B is the Boltzmann constant, ϑ is the temperature in Kelvins, N is the number of chains in the network of a cross-linked polymer

tests, both intrinsic and extrinsic factors can greatly influence the testing results of in vitro studies. In such studies, the tissues are usually analysed in extreme conditions exploring their maximum stretch or compression that are impossible to study in vivo. In in vivo experiments, indentation is often employed as a non-invasive method to measure the soft tissue's response [6]. It is a common practice for an indentation depth to be limited by a pain tolerance threshold for in vivo experiments [7], with cases of pain tolerance explored as well [8]. Although the reported pain levels vary significantly among participants due to the individuals' characteristics, similar regions exhibit similar behaviours.

The main challenge of studies of human tissues in vivo is the necessity of involvement of human participants. Mostly, conventional experimental equipment is not suitable to carry out the measurements needed for the studies, so custom testing rigs and sensors are usually developed [4,9,10]. This equipment needs to produce accurate results while complying with strict safety regulations, so that the participants are not in risk during the examination. Ethical regulations for the methodology also should be followed. Hence, in vivo studies can be a very challenging process. Computational modelling can be a useful substitute as it provides tools to test hypotheses and predict the mechanical behaviour without the need for human involvement, thus eliminating the risk for accidents. It also constitutes an ideal method for parametric studies based on multiple repetitions needed to study the effects of various parameters and their combinations.

To predict the soft-tissue behaviour, a finite-element method (FEM) has been extensively used. Both 2D and 3D models were developed to capture spatial distributions of deformations and pressure in the tissues [11]. Taking advantage of a smaller number of elements and the lower computational cost, 2D models were used to introduce various properties of the analysed tissues. The assumptions employed in this simplified modelling approach can significantly affect the modelling strategy and the obtained results thus requiring further detailed investigations [12].

Taking advantage of the computational power that become available in the recent years, bigger and more complex models were developed, including full-limb models with patient-specific anatomical and morphological features. These developments were supported by the use of magnetic resonance imaging techniques for better accuracy of the measurements and identification of individual tissue's behaviour [13–15]. Stress distributions on the surface and inside the tissues were studied with the FEM together with interactions between tissues and external parts such as prosthetic sockets [16,17].

Although the model geometry is becoming more and more complicated and patient-specific, still little is known about the material behaviour of soft tissues. Although describing their mechanical behaviours is an active field of research, with many variants of constitutive models reported in the literature. Initial approaches that used linearly elastic material models were quickly phased out due to their limited suitability for cases with large deformation and material's nonlinearity [18]. Various hyperelastic models were proposed for more adequate description of tissue's deformations. In these models, the strain energy of a solid is expressed as a function of the invariants or principal stretches, with the stresses calculated with the proper derivation. Such models are introduced in Table 1.

Identifying the in vivo material parameters for soft tissues is an important but challenging aspect of experiments. When testing rigs are available, an inverse engineering approach can be employed to fit the computed results to the respective experimental data [20,21]. Despite a significant number of studies carried

out in this field, there is still no established universal model developed for soft tissues, while the respective material parameters characterising their mechanical behaviour have significant variations. As a result, the existing models are mostly limited to subject-specific studies and local behaviour. A summary of the material parameters reported in the literature for limb's soft tissues is presented in Table 2.

Various methods were employed to model the soft tissue. Initially, single-domain models (i.e. with one bulk tissue throughout its volume) were common, usually with linear elastic or Neo-Hookean material formulation of their mechanical behaviour [17,66]. The schemes with multiple domains, presenting skin, fat and muscle tissues separately, were also developed; they mostly considered the skin and fat tissue as a joint domain due to their similar morphological character in clinical images. More recent studies investigated the necessity of including further features in the model, such as fascia, veins and individual muscle compartments, but there was no (or very limited) information about the response of these individual materials [23,67].

This study, focused on a numerical approach, aims to investigate and identify a necessary size of a 3D FE model for simulation of indentation of a human lower limb. In addition, the effect of the chosen levels for material parameters was investigated after the optimal model size was identified. The effect of the loading direction was also assessed.

2 Development of FEA model

One of the challenges that arise when modelling human soft tissues is unique anatomical characteristics of every individual, as mentioned above. To keep analysis consistent, in this study, a contour of a human thigh was manually segmented from a transverse-cut medical image (Fig. 1) and used for all subsequent assessments. Contours of a bone and a dermal tissue of the modelled thigh were also identified and separately segmented using NX 11.0. A skin and an adipose tissue were segmented as single part, as reported in previous studies [67]. A final sketch of the limb including three types of tissue (bone, muscle, dermal), each as a separate domain, was then imported into ABAQUS 2018 CAE software for analysis.

The size of the thigh was scaled according to the average size of male's European human thigh circumference as in Table 3, and the transversal cross section was extruded along the main (bone) axis, as in the previous approach [47]. The length of the extrusion was determined based on requirements of the subsequent analysis. Each tissue's region (domain) was partitioned to introduce the respective material properties. The mesh was created using 4-node linear tetrahedral elements with hybrid formulation (C3D4H), and mesh convergence was achieved with an approximate node spacing of 3 mm at the outer site and 5 mm at the bone region. A cylindrical, flat-ended indenter with diameter of 10 mm, with an edge radius of 1 mm, was modelled as analytical rigid surface. To implement the indentation simulation, the bone section was fully constrained, while the indenter's flat end was positioned in contact with the skin and allowed to translate axially towards the centre of the bone. The selected friction coefficient was 0.5 and used for all the models developed (see also Sect. 2.2).

2.1 Constitutive model

The soft tissues' nonlinear behaviour in our simulations was described using the Ogden hyperelastic model for incompressible materials [72]. In an isotropic, first-order Ogden model, the strain energy W is given as a function of the principal stretches (see Eq. (2) in Table 1). In this equation, N represents the number of terms used in the strain energy function, μ_p are components of shear moduli and α_p are dimensionless constants. The classical shear modulus μ can be obtained in the reference configuration from

$$2\mu = \sum_{p=1}^{N} \mu_p \alpha_p, \quad \mu_p \alpha_p > 0, \, p = 1, \ldots, N \tag{8}$$

while the three principal Cauchy stresses σ_α are given by

$$\sigma_\alpha = -p + \sum_{p=1}^{N} \mu_\alpha \lambda_\alpha^{\alpha_p}, \quad a = 1, 2, 3 \tag{9}$$

Material parameters selected for the two hyperelastic tissues used in this study are highlighted in bold font in Table 2 describing the average reported material stiffness. Linear elasticity was used for the bone, with

Table 2 Hyperelastic models used to model soft tissue in different schemes and values of their parameters as well as experimental data for elastic properties

Constitutive model Ogden 1st order	Material parameters		Numerical model	Comments	References
	μ (kPa)	α			
Skin	0.01	26	F		[22]
	5.22	7.49	A, D	*	[21]
	6.568	**25.152**	F	(u)	[20]
	2.6–39.8	33.452–35.993	F	(u)	[23]
	10	26	A, D		[24]
	110	9			[25]
Fat	16.53	0.77	A, D		[24]
	0.02353	12.066	H		[26]
Muscle	5.2	4.78	A, D		[21]
	10.2–21	**15.7–27.1**	F	Rats in vivo, +	[27]
Soft tissue	3.65	5	A, C	Rats in vivo, +	[28,29]
	1806	9.78	B, C		[30]
Ogden 2nd order	μ (kPa)	α			
Skin	27.039	3.786	F	(u)	[20]
	2.769	39.378			
Fat	-4.629×10^{-9}	-16.829	F		[26]
	-1.613	-1.043			
Linear elastic	E (kPa)	v			
Skin	14	-	E	In vitro, (u)	[31]
	2-35	-	N/A		[12,32]
	30-33	0.3–0.4	E		[32]
	100	–	N/A		[33]
	41–365	–	F	(u)	[34]
Fat	0.8–18.1	–		*	[35]
Muscle	80	–	N/A		[12,32]
Soft tissue	100	0.1–0.5	E		[4]
	100	0.49	A, C		[36]
	160–260	0.49	A, C		[18]
	200	0.49	A, C		[37–40]
	200	0.475	A, C		[41]
	200–250	–	A, C		[42]
	–	0.4925	F	Stiffness = 6kPa	[43]
	965	0.45	A, C		[44]
	300–150,000	0.45	A, C		[45]
	32.1	–	A, C		[46]
Neo-Hookean	C_1 (kPa)	k (kPa)			
Skin	N/A		E, G		[47,48]
	13.91–17.21	–	B, D		[49]
	0.37–1200	35.1–30,880	F		[15]
	2000	30,000	G		[7]
	–	3000	A, D		[50]
Fat	2–7	71.3–140	F		[11]
	–	36	A, D		[50]
	1	36	G		[8]
	–	–	E, G		[47,48]
	0.8	–	F		[51]
	927.94	–	B	*	[52]
Muscle	25.5	–	A, D		[16]
	3.37–4.07	–	B		[49]
	9.4–12.9	61–78	F		[11]
	–	0.881–1.032	B, D		[52]
	2.9–5.55	1.06–1.16	A, C		[53]
	5.952	92.8	G		[7,8]
	1.75	–	F		[51]
	–	116	A, D		[50]
	440.712	–	B, D		[52]
Soft tissue	2–100	–	F, G		[54]

Table 2 continued

Constitutive model Ogden 1st order	Material parameters			Numerical model	Comments	References
	μ (kPa)	α				
Mooney–Rivlin	**C_{10} (kPa)**	**C_{01} (kPa)**	**D_1**			
Skin	0.186	0.178	–	A, D		[55]
	5.8–13	22–142	–	E		[56]
	9.4	–	0	A, D		[46]
	300	0	–	N/A		[25]
	0.4–148.9	0–82	–	A, D	Scar tissue included	[16,46]
Fat	0.143	0	70.2	A, D		[46]
	0.19	0.18	–	A, D		[55]
Muscle	4.25–8.075	0	1.243–2.36	A, D		[46]
	0.12	0.25	–	A, D		[55]
Soft tissue	85.5	21.38	–	A, C		[14]
James–Green–Simpson	**C_{10} (kPa)**	**C_{01} (kPa)**	**C_{11} (kPa)**			
Soft tissue	2.6	0.64	5.7	A, C		[57]
	N/A			A, C & E		[2]
Measurements of Shear modulus	**μ (kPa)**					
Muscle	4.5–6.6				(u)	[58]
	6–8					[59]
	6–13					[60]
	7.5–15.1				(u)	[61]
	3.75–6.6					[62]
Fat	2.92–3.16					[62]
Measurements of Elastic Modulus	**E (kPa)**					
Skin	11–120				(u)	[63]
	20–100				(u)	[64]
	420–820				(u)	[65]
	1120				(u)	[66]

A: Full-limb model, B: Local area, C: Single-material, D: Multi-material, E: Axisymmetric, F: Simplified, G: Extrusion. (+) indicates animal tissue, (u) indicates upper-limb tissue, (*) indicates that skin and fat tissue are considered as one. Bold values were used for material properties in this study

the Young's modulus of 20 GPa and the Poisson's ratio of 0.3. All the modelled tissues were assumed to be homogeneous and isotropic materials.

A preliminary numerical study was undertaken to assess the effect of friction at the indenter/limb interface in a broad range of the coefficient of friction. Eventually, the magnitude of 0.5 was chosen for this parameter in the main study to emulate conditions of the dry-skin examination.

2.2 Study of model size

As well known, a type of boundary conditions has a significant impact on the accuracy of simulation results. While simulating indentation of a human limb can be captured relatively accurately with a larger size of the limb, it may not be necessarily viable for multi-model and/or parametric studies. Therefore, in this study, indentation characteristics at two different sites—Site A (with soft-tissue thickness of 47 mm) and Site B (87.5 mm) (Fig. 2b)—were evaluated with models with varying length: from 20 to 220 mm (Fig. 2a). The simulations were performed with both an unconstrained and a fully constrained boundary conditions applied at both transversal ends (full cross sections) of the limb. Convergence was assumed when the difference in the reaction force between the models with the unconstrained and fully constrained boundary conditions was smaller than 5%.

For Site A, with tissue thickness of 47 mm, convergence in the resulting reaction force was achieved for a model length of 80 mm, while for Site B (thickness 87 mm) this happened at 150 mm (Fig. 3)., A ratio of 1.7 between the minimum model length and the tissue thickness was found for both cases. Considering this ratio, the main study was implemented with two different models, each with the minimum identified size.

Fig. 1 Anatomy of human femur [68]

Table 3 Average size of thigh's circumference of healthy adults for various geographical regions

	Men	Women	References
Europe	56.6 ± 4.6 cm	59.6 ± 5.2 cm	[69]
Denmark	55.5 ± 7.0 cm	57.5 ± 9.0 cm	[70]
North America	63.1 ± 5.3 cm	65.5 ± 9.2 cm	[71]
South Korea	53.9 ± 5.3 cm	51.8 ± 5.7 cm	[72]
Taiwan	50.7 ± 5.0 cm		[73]
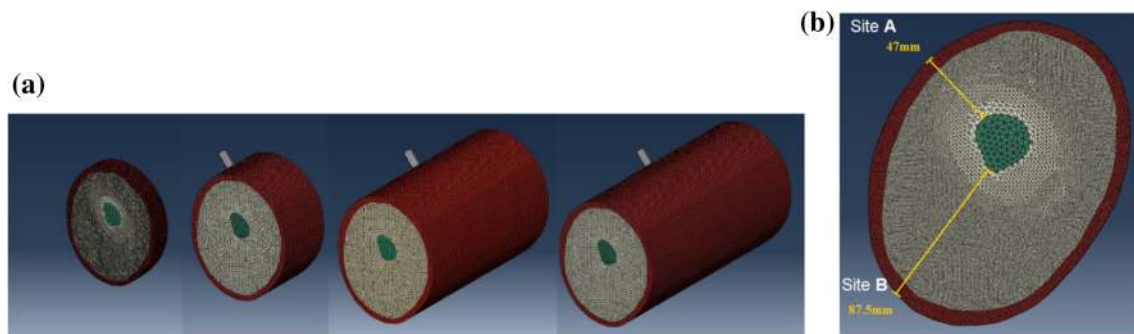
Fig. 2 a Models with length of 20, 60, 150 and 220 mm. **b** Indentation sites used in model corresponding to minimum and maximum tissue thicknesses

3 Methodology

3.1 Effect of loading direction

When performing and simulating indentation, ideally, the indenter's axis should pass through the bone's centre. Obviously, small misalignment can occur in real-life experiments as a result of the unique feature of individuals or a human error. A set of indentations was simulated for various loading directions on Sites A and B, to examine the sensitivity of the indentation protocol to the misalignment of the indenter and the significance of the internal geometry of the limb. Effects of both linear and angular misalignments were investigated. An angular misalignment of 10° was considered for both clockwise and counter-clockwise directions. On the
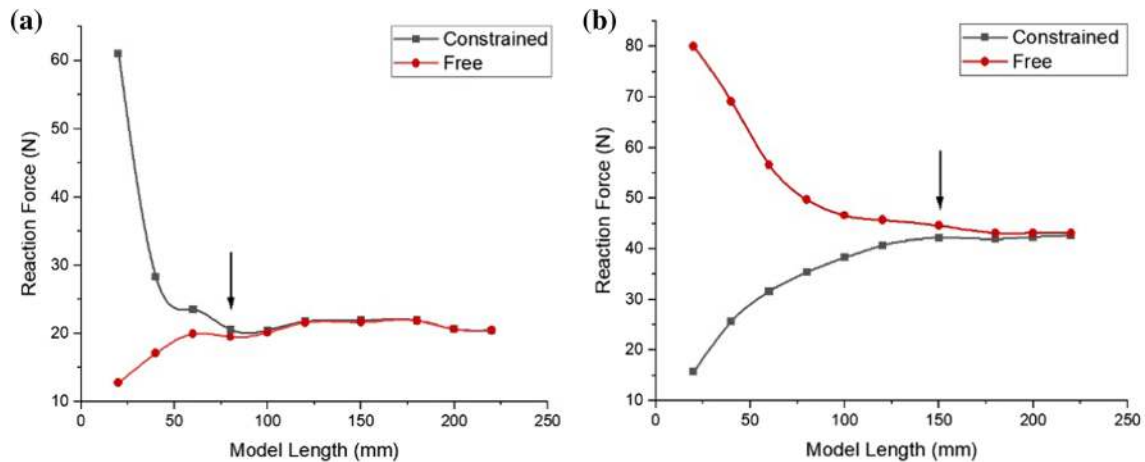
Fig. 3 Reaction forces for models with various lengths and constrained and free ends for Site A (**a**) and Site B (**b**) (The arrow shows the convergence point)

thinner Site A, the indentation axis was still meeting the bone tissue for the entire range of this misalignment, while on the thicker Site B, the axis was off the bone. To study the effect of linear misalignment, the indenter was repositioned at ± 5, ± 10 and ± 20 mm parallel to the original position. The original and new indentation directions are shown in Fig. 3. For this study, the models optimal identified for each site (as discussed above) were used.

3.2 Effect of material parameters

In this study, the soft-tissue response was investigated for various sets of material parameters for the first-order Ogden hyperelastic model (see Sect. 2.2). A broad range in properties' magnitudes available in the literature necessitated the assessment of the respective effect. In our numerical simulations, changes in material properties were limited to the domain of muscles that constituted the largest part of the modelled soft tissue, whereas those of the skin and adipose were kept at the same level. In reference to the initial set of material parameters—Set R in Fig. 5, additional sets were created to explore the changes in the limb's response to indentation. Two additional levels were introduced for μ, the first equal to one half of the reference value and the second was three times higher than the reference. For α, a nearly fivefold decrease of the reference magnitude was used, with the total range being from 4.5 to 21.4. Permutation of these magnitudes resulted in five additional sets of material parameters presented in Fig. 5. So, Sets 2 and 4 have the same level of α as Set R, while differing in the magnitude of μ: Set 2 has the lowest one, while Set 4—the highest. Sets 1, 3 and 5 share the same—lowest—magnitude of α, with Set 3 retaining the reference level of μ, while Sets 1 and 2 having the same lowest level of μ and Sets 4 and 5—highest μ.

Levels of the reaction force at the indenter tip, obtained in numerical simulations, were compared for all the sets, with their ratios used to evaluate the contribution of each parameter. The aim of this part of the study was to identify the range of the expected reaction forces for the specific choice of material parameters and to assess the ability of this formulation to capture the tissue response during indentation.

3.3 Axisymmetric model

An axisymmetric finite-element model was also developed, with the same geometrical features of the limb tissue. A rectangular domain with width of 40 mm and height of 47 mm, with the latter coinciding with the symmetry axis, was created for simulations of indentation at Site A. Its bottom edge was fixed in all degrees of freedom, representing the tissue attached to the bone, while the edge of the tissue parallel to the symmetry axis was left free. Indentation to the depth of 20 mm was modelled, using an indenter identical with that in the 3D limb model. To elucidate the mechanical behaviour of the soft tissue, it is necessary to assess the contribution of the bone to the stresses so that the measurements present the data for the material of interest rather than a
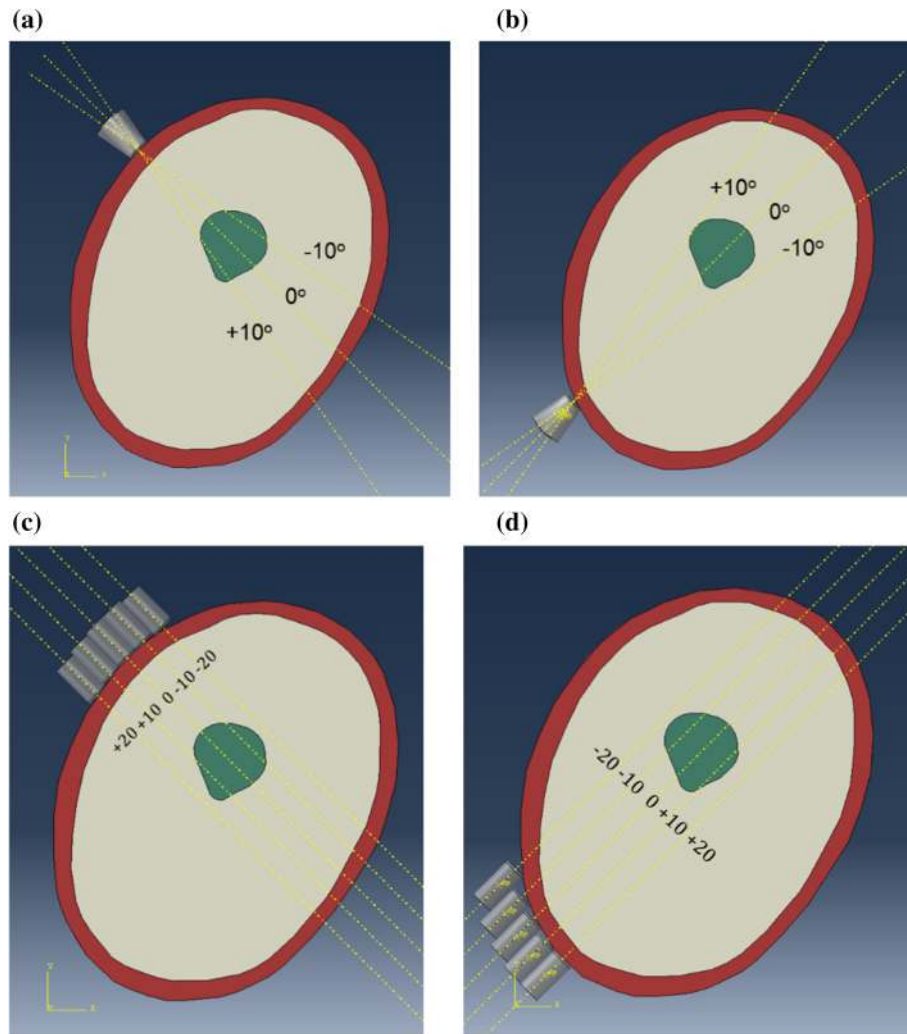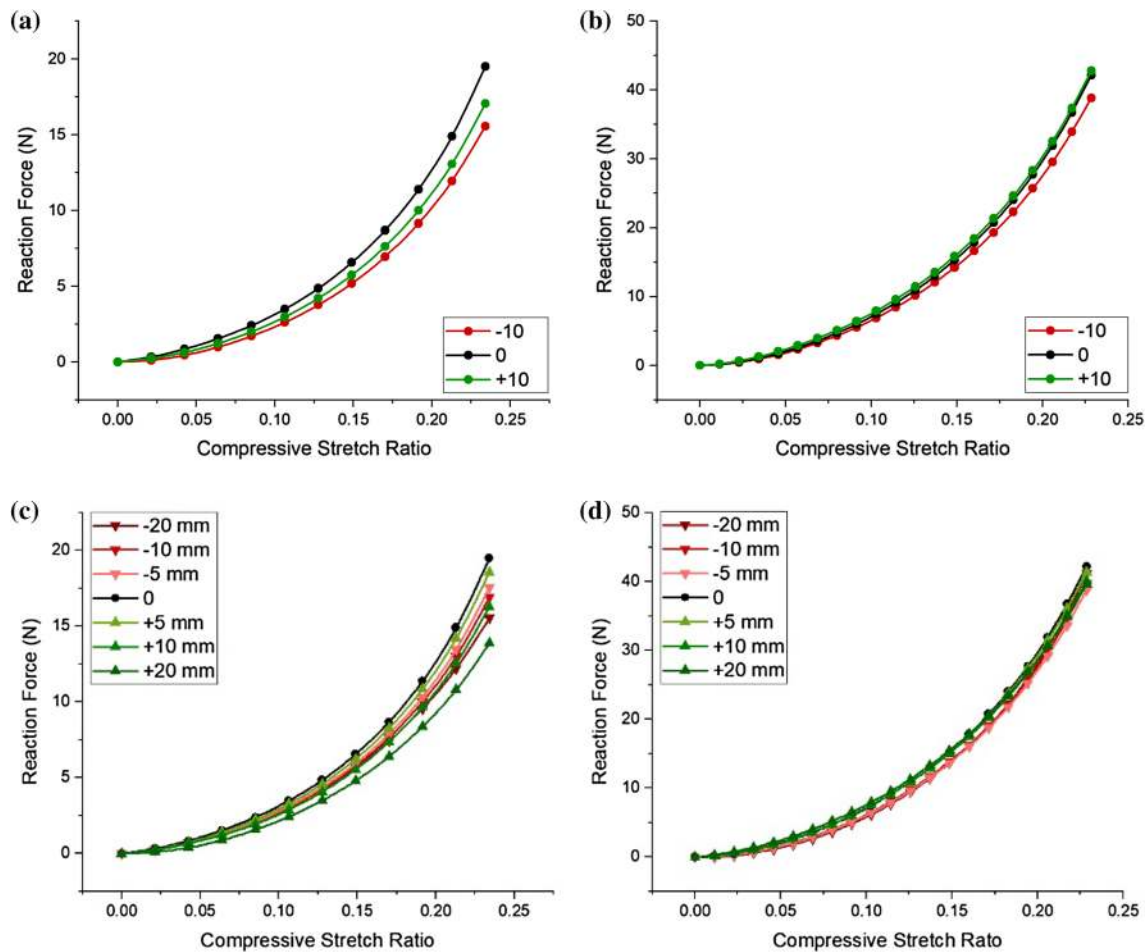
Fig. 4 Angular misalignments on Site A (**a**) and Site B (**b**). Linear misalignments on Site A (**c**) and Site B (**d**)
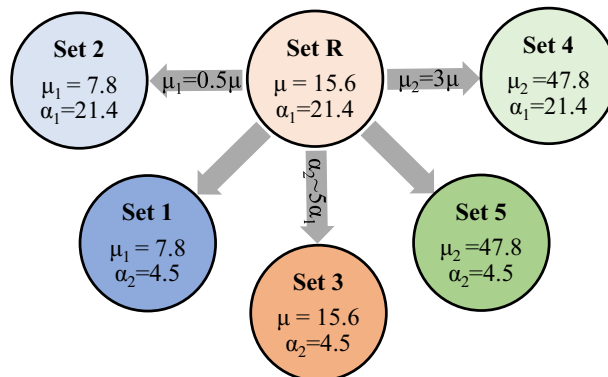
Fig. 5 Sets of material parameters used for muscle domain in simulations (Set R represents the reference values; μ is in kPa.)

Fig. 6 Evolution of reaction force against compressive stretch ratio (ratio of indentation depth to tissue thickness): effect of angular misalignment for Site A (47 mm) (**a**) and Site B (87.5 mm) (**b**); effect of linear misalignment for Site A (**c**) and Site B (**d**)

combined data for the limb. The minor principal strain was chosen for comparison as it describes compressive strains of the material under the indenter tip.

4 Results

4.1 Effect of angular misalignment

The results calculated for the cases of angular misalignment presented significant differences. In both sites examined, the difference in reaction forces for the misaligned directions and the reference exceeded the 5% threshold used throughout the simulations. Specifically, a ±10° misalignment of the indenter tip at Site A resulted in 25.3% (+10%) and 14.4% (−10%) reductions in the peak reaction force, respectively, with a slight difference as a result of non-symmetric limb profile. For Site B (thicker), the resulting force was 8.6% (+10%) lower and 1.4% (−10%) higher than the original value, (Fig. 6a, b). The results indicate that the reaction force measured in indentation is sensitive to the alignment and structure of the underlying tissue, while the thicker layer of the tissue helps to mitigate some of the misalignment effect.

Table 4 Difference in reaction force (%) for various indentation directions at maximum indentation depth 20%

	−20 mm	−10 mm	−5 mm	−10°	0	+10°	+5 mm	+10 mm	+20 mm
Site A	−20.24	−13.25	−9.87	−25.3		−14.4	−4.67	−16.42	−28.86
Site B	−2.34	−5.60	−8.07	1.4		−8.6	−2.01	−4.94	−6.05

4.2 Effect of eccentricity

The study of the effect of eccentricity to the indentation direction demonstrated the growing distance from the ideal direction (i.e. to the bone centre) caused a monotonous decrease in the reaction force. The maximum decline in this force measured for a 20 mm offset at Site A exceeded 20% for both directions (Fig. 6c). For smaller offset positions, the positive offsets, at +5 mm and +10 mm, seem to have less effectiveness compared with the negative offsets.

The extent of reduction in the maximum reaction force at site B was generally lower. Besides, the diminishing trend was observed only for the positive offset distance, while for the negative one it was inversed (Fig. 6d and Table 4). The difference between these two cases was attributed to a rapid change in the thickness and curvature of the soft tissue as the offset changed from −20 to +20 mm.

4.3 Effect of material parameters

Since both constitutive parameters of the first-order Ogden model affect directly the shear modulus, an increase in either of them resulted in an increased reaction force, as was demonstrated by numerical simulations. Still, as a result of their different roles in the constitutive equation (see Eq. 9), contribution of μ was noticeable throughout the entire modelled stretching. On the other hand, parameter a contributed more to the response after the compressive stretch ratio exceeded 0.1 for both Site A and Site B (Fig. 7). Thus, μ defined the slope of force-stretching curves at the early stage of the process.

Analysis of the results for Site A (Fig. 7a) demonstrate that changes in μ resulted in almost proportional variations in the reaction force for compressive stretch ratio above 0.15. Specifically, at compressive stretch ratio of 0.2, the ratio of reaction forces for Set 2 and Set R (i.e. the same α) was 0.58, while that for Set 1 and Set 3 (i.e. the same, but lower α) was 0.61. For the same loading conditions, the ratio of reaction forces for Set 4 and Set R (at constant α) was 2.56, while that for Set 5 and Set 3 was 2.68. A change in the magnitude of α from 4.5 and 21.5 for the same level of μ returned continuously a reaction force around 1.5 times larger at stretch ratio of 0.2.

Similarly, the relationship between the reaction forces for various sets of material parameters for Site B (Fig. 7b) followed the same trends as in Site A. The ratio of reaction forces for Set 2 and Set R was 0.53 at compressive stretch ratio of 0.2, while that for Set 4 and Set R was 2.7. For the lower level of α, the ratios for forces for Set 1–Set 3 was 0.55 and for Set 5 to Set 3 was 2.65, respectively. At compressive stretch ratio
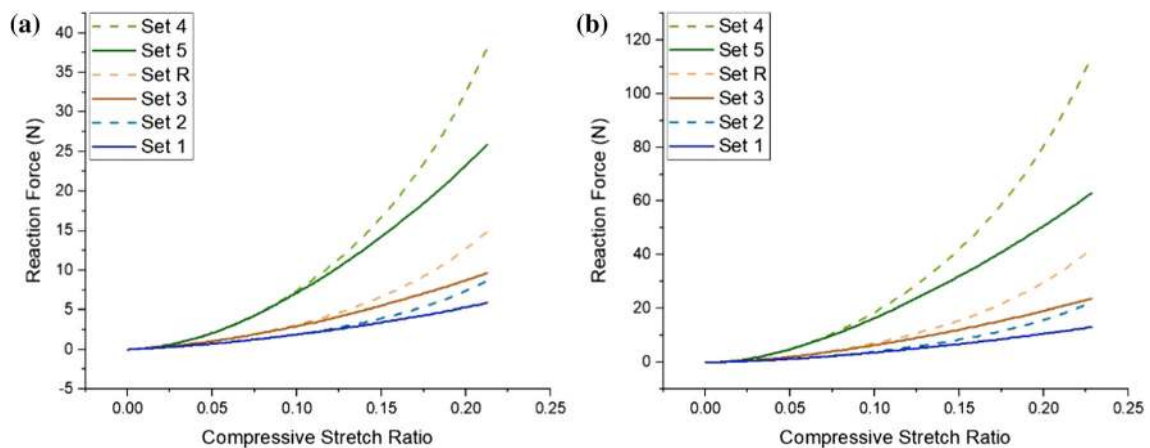

Fig. 7 Evolution of reaction force for studied material sets for Site A (47 mm) (**a**) and site B (87.5 mm) (**b**)

of 0.2, the variation of α resulted again in the approximate ratio of 1.5 for forces in materials with the higher level of α.
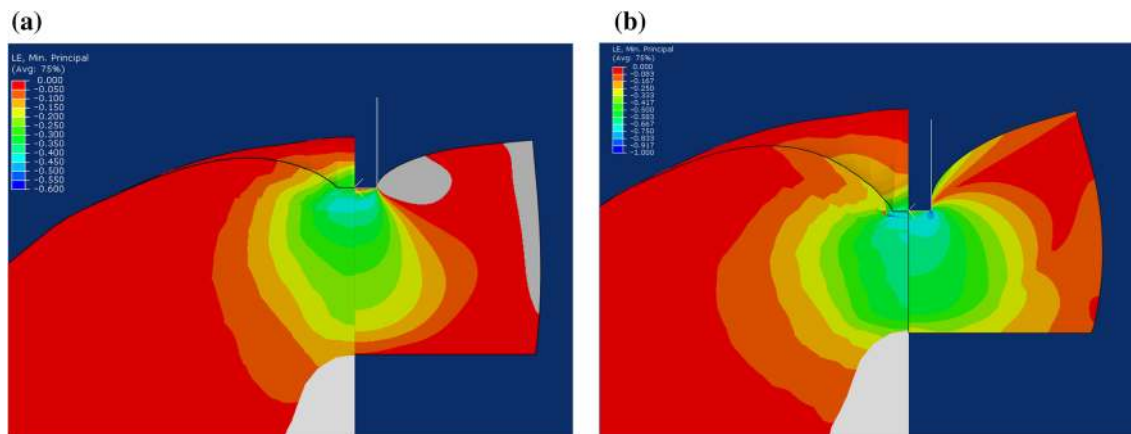
4.4 Comparison with axisymmetric model

A detailed comparison between the 3D limb model and an axisymmetric one was made using the reference set (Set R) of material parameter from Fig. 5. For direct comparability, both models had the same ratio of the length to the tissue thickness (equal to 1.7) identified earlier in the study of the model size (Sect. 2.2). The boundary conditions at the edges of the models were free for all six degrees of freedom since the stress concentration disappeared fully at these dimensions.

A good agreement was revealed, notwithstanding differences in geometry, boundary conditions and domain shapes. Good accordance for evolution of the reaction force with indentation depth was observed for the entire loading process as shown in Fig. 8. In addition, distribution of a principal compressive strain at 10 mm and 20 mm indentation displacement were also compared (Fig. 9), with good compliance both for the character of distribution and the magnitude. So, despite the existence of a continuous dermal layer in the three-dimensional limb model, the material response could be captured highly accurately with the simplified axisymmetric model during the entire process of indentation.
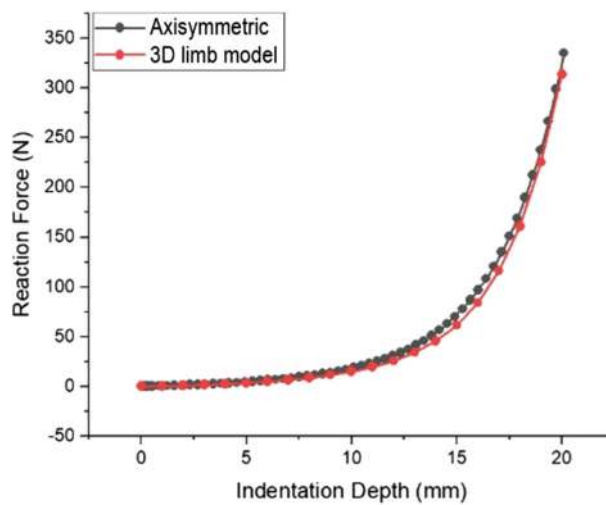
Fig. 8 Comparison of force–displacement curves for 3D model (Site A) and corresponding axisymmetric model for reference material parameter set (Set R: $\mu = 15.6$ kPa; $\alpha_1 = 21.4$)

Fig. 9 Comparison of principal logarithmic strains for 3D full-limb and axisymmetric models for Site A (47 mm) for various indentation depths: **a** 10 mm; **b** 20 mm
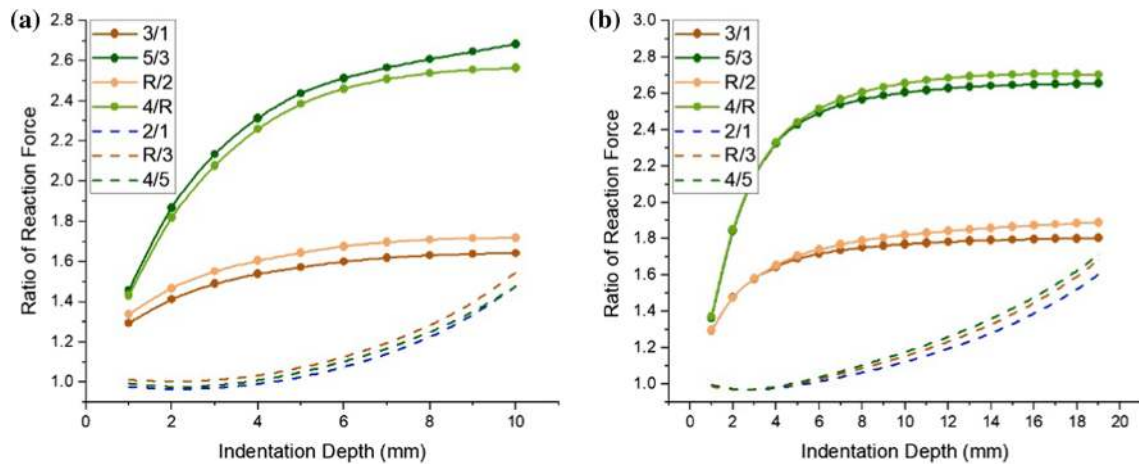
Fig. 10 Ratio of reaction force for various sets of material parameter (see notation in Fig. 5) at different indentation depths: **a** Site A; **b** Site B. Solid lines are used for comparisons of sets with the same α; dashed lines—with the same μ

5 Discussion

It is evident that a small misalignment of the indenter can result in significant differences in the resulting force–displacement curves, and, therefore, influence the quality of experimentally obtained data. So, when performing an indentation experiment using a flat indenter tip to extract force–displacement data with an inverse analysis, it is important to simulate the exact position and direction of the indenter, instead of using idealised boundary and loading conditions. A recent study on rat tibia [27] concluded that tests with a spherically shaped indenter along various indentation directions altered the strain distribution within a defined volume of tissue.

However, reaction forces of the primary measurement were not reported, so further experimental investigation is necessary to assess differences between their testing protocol and the idealised modelling.

As demonstrated, the changes in material parameters of the first-order Ogden hyperelastic model significantly influenced the evolution of reaction force with the indentation depth. The extent of the effect of material properties varied for specific regions. In order to elucidate the contribution of each parameter, the ratios of reaction forces for the same sets of μ (or α) with different levels of α (or μ) were compared (Fig. 10) for both Site A and Site B using the sets of material parameters introduced in Sect. 3.2 (Fig. 5). The effect of changing the shear modulus was evident throughout the entire deformation process, starting at around 1.4 at the initial loading stage, but quickly saturated to around 2.6 for the ratio $\mu = 3$ (1.6 for $\mu = 2$) at larger indentation depths (Fig. 10a, solid lines). In contrast, the contribution of α was mostly negligible up to the indentation depth of some 10% of the initial thickness of the soft tissue (Fig. 10a, dashed lines). Interestingly, it was also revealed that these ratios were mostly unchanged for Site B, suggesting thickness-independent tissue responses.

It is important to recall at this point that since only the muscle material parameters were changed, the case with Set 1 can effectively be considered as single-material tissue since the muscle properties were almost identical to those of the layer of skin and adipose. Although the reference material, Set R, is stiffer than that corresponding to Set 2 (Fig. 7), no significant differences in the behaviour was observed as a result of introduction of the skin/adipose domain. The response followed a similar trend although with a different magnitude.

The model was further compared with specially performed experimental indentation tests of a human calf with the same range of tissue thicknesses (its detailed experimental protocol and results will be discussed in a separate paper). Although this comparison is suitable only for preliminary conclusions, it was evident that the model can reproduce the experimentally observed behaviour of soft tissues at large indentation depths (Fig. 11). A significant extent of variability in mechanical behaviours of lower-limb soft tissue is obvious, especially for the cases of tissue with the same thickness (58.8 mm) in different persons, proving the difficulty of studying these materials. The comparison of the obtained numerical results with the experimental response suggested that many modelling assumptions resulted in overestimation of the soft-tissue stiffness. Considering more recent studies focusing on measuring mechanical properties [57–65], a lower range of elastic moduli was reported (see Table 2). It is thus important to consider lower values for material parameters that correspond to
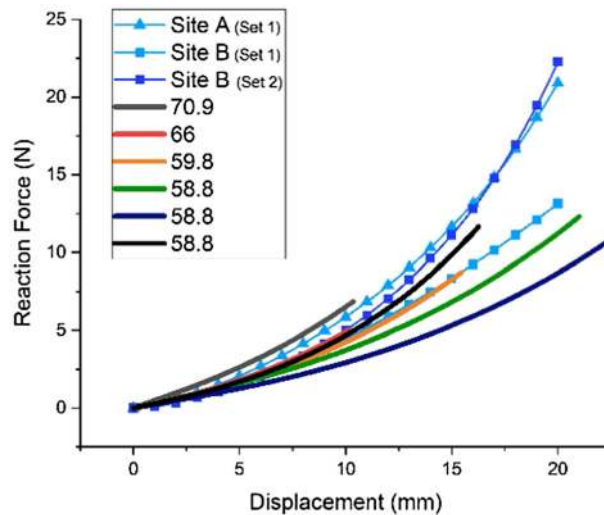
Fig. 11 Comparison of experimental data for indentation of calves with different thickness (solid lines; the legend provides the soft-tissue thickness in mm) and simulation results (lines with markers)
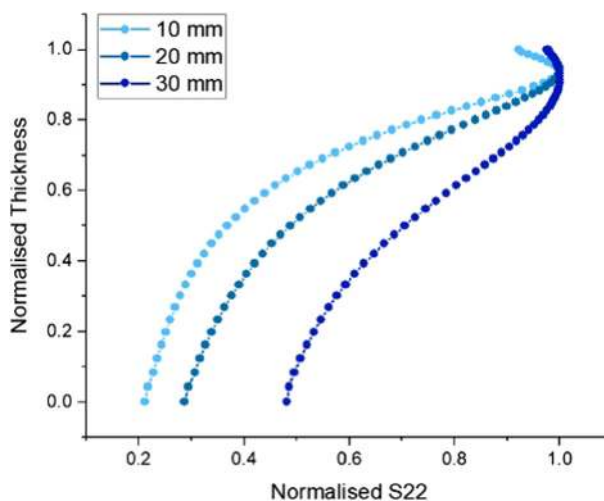
Fig. 12 Distribution of normalised stress in indentation direction along tissue thickness

lower elastic moduli for thick muscles. These values should be also considered as a reference point in future modelling attempts.

Although the indentation experiments were used extensively to characterise the in vivo soft tissue behaviours of the lower limb, there were only a few studies that investigated the distributions of stress and strain in the tissue directly beneath the indenter. Also, there was no information regarding the reaction contribution of the rigid support to the tissue's response in the indentation process. Furthermore, computing hyperelastic material properties based on the assumption of a quasi-statically, uniformly deformed tissue would be an oversimplification. To elucidate the stress development directly beneath the indenter tip, the normalised (with its peak magnitude) stress in the direction of indentation for different indentation depths (10 mm, 20 mm and 30 mm) was plotted along the normalised tissue thickness for Site A in Fig. 12. The results demonstrated a significant variation of stress along the indentation direction. For indentation depth of 10 mm and 20 mm, less than half of the thickness was affected by stress in excess of 50% or the peak stress concentrated at the top of the tissue. On the contrary, for a higher indentation depth (30 mm), the stress concentration band at the upper tissue was much larger, with some 90% of the thickness exposed to higher stresses (i.e. exceeding 50% of the peak stress). This is an indication that the properties measured at this depth were affected by the rigid support (bone), suggesting that the maximum indentation depth for studying this tissue should be limited to 0.45 of

its original thickness. A further study on the link between the material stiffness and the indentation depth is currently under progress.

6 Conclusions

In this paper, various modelling strategies for numerical simulations of indentation on human lower-limb soft tissue were suggested and evaluated. A consistent minimum size of the model was established based on the ratio between the model length and the tissue thickness, so that the simplified boundary conditions in 3D and axisymmetric models can be used. For analysis of hyperelastic materials and the indentation depth up to 20% of the initial thickness of soft tissue, a ratio of 1.7 between the model length and the tissue's thickness can be assumed to satisfy sufficiently the Saint-Venant's principle.

It was also evident that the indentation reaction force was sensitive to the indentation direction and the indenter's initial position with respect to morphological features of the tissue (e.g. the bone shape). A further experimental study is needed to accurately quantify this effect; obviously, the precise alignment of the indenter in experimental procedures is advisable to avoid potential errors.

The findings of this study further revealed that the mechanical response to indentation of the lower-limb soft tissue was affected differently by the two parameters of the first-order Ogden hyperelastic material model. The shear modulus is proved to contribute significantly at all the stages of the material's deformation, while α was mostly contributing to the nonlinear behaviour for deeper indentations. The ratios material parameters for different sets indicated that the difference in reaction force due to changes in shear modulus remained constant once the indentation depth reached around 10% of the soft-tissue's initial thickness. For the inverse analysis, it is suggested that hyperelastic materials described by this formulation could have the material parameters identified individually, reducing the computational cost of multi-parametric optimisation. The shear modulus can be identified by shallow indentation tests ($< 10\%$) for a given α. Once the slope of the curve is identified, the level of α can be calibrated for the obtained shear modulus. Assessment and comparison of the calculated distributions for compressive stress and strain under the indenter for 3D and axisymmetric models suggested that hyperelastic materials can be characterised reasonably accurately for stretch ratios up to 0.45, without being affected by reaction of the rigid support (bone).

In conclusion, this study indicated the parameters necessary for modelling the indentation processes of human soft tissue. The results—also compared with experimental data—agree with the literature but also indicate that further studies should be carried out to advance the existing modelling strategies. There are also opportunities to further enhance numerical models by employment of material formulations for soft tissues, accounting directly for the effect of fibres (see e.g. [74–76]).

References

1. Holzapfel, G.A.: Biomechanics of soft tissue. In: Krempl, E., Ho, K. (eds.) Handbook of Materials Behavior Models, pp. 228–253. Academic Press, Cambridge (2000)

2. Tönük, E., Silver-Thorn, M.B.: Nonlinear elastic material property estimation of lower extremity residual limb tissues. IEEE Trans. Neural Syst. Rehabil. Eng. **11**, 43–53 (2003). https://doi.org/10.1109/TNSRE.2003.810436

3. Fung, Y.C., Cowin, S.C.: Biomechanics: mechanical properties of living tissues, 2nd ed. J. Appl. Mech. **61**(4), 1007 (1994). https://doi.org/10.1115/1.2901550

4. Mak, A.F.T., Liu, G.H.W., Lee, S.Y.: Department of veterans affairs biomechanical assessment of below-knee residual limb tissue. J. Rehabil. Res. Dev. **31**, 188–198 (1994)

5. Pierrat, B., MacManus, D.B., Murphy, J.G., Gilchrist, M.D.: Indentation of heterogeneous soft tissue: local constitutive parameter mapping using an inverse method and an automated rig. J. Mech. Behav. Biomed. Mater. **78**, 515–528 (2018). https://doi.org/10.1016/j.jmbbm.2017.03.033

6. Bader, D.L., Bowker, P.: Mechanical characteristics of skin and underlying tissues in vivo. Biomaterials **4**, 305–308 (1983). https://doi.org/10.1016/0142-9612(83)90033-9

7. Finocchietti, S., Takahashi, K., Okada, K., Watanabe, Y., Graven-Nielsen, T., Mizumura, K.: Deformation and pressure propagation in deep tissue during mechanical painful pressure stimulation. Med. Biol. Eng. Comput. **51**, 113–122 (2013). https://doi.org/10.1007/s11517-012-0974-9

8. Finocchietti, S., Nielsen, M., Mørch, C.D., Arendt-Nielsen, L., Graven-Nielsen, T.: Pressure-induced muscle pain and tissue biomechanics: a computational and experimental study. Eur. J. Pain **15**, 36–44 (2011). https://doi.org/10.1016/j.ejpain.2010.05.010

9. Klaesner, J.W., Commean, P.K., Hastings, M.K., Zou, D., Mueller, M.J.: Accuracy and reliability testing of a portable soft tissue indentor. IEEE Trans. Neural Syst. Rehabil. Eng. **9**, 232–240 (2001). https://doi.org/10.1109/7333.928583

10. Zhang, M., Zheng, Y.P., Mak, A.F.T.: Estimating the effective Young's modulus of soft tissues from indentation tests— nonlinear finite element analysis of effects of friction and large deformation. Med. Eng. Phys. **19**, 512–517 (1997). https://doi.org/10.1016/S1350-4533(97)00017-9

11. Avril, S., Bouten, L., Dubuis, L., Drapier, S., Pouget, J.F.: Mixed experimental and numerical approach for characterizing the biomechanical response of the human leg under elastic compression. J. Biomech. Eng. (2010). https://doi.org/10.1115/1.4000967

12. Pailler-Mattéi, C., Zahouani, H.: Study of adhesion forces and mechanical properties of human skin in vivo. J. Adhes. Sci. Technol. **18**, 1739–1758 (2004). https://doi.org/10.1163/1568561042708368

13. Portnoy, S., Siev-Ner, I., Shabshin, N., Kristal, A., Yizhar, Z., Gefen, A.: Patient-specific analyses of deep tissue loads post transtibial amputation in residual limbs of multiple prosthetic users. J. Biomech. **42**, 2686–2693 (2009). https://doi.org/10.1016/j.jbiomech.2009.08.019

14. Ming Zhang, C.R.: Comparison of computational analysis with clinical measurement of stresses on below-knee residual limb in a prosthetic socket. Inf. Process. Lett. **113**, 849–851 (2013). https://doi.org/10.1016/j.ipl.2013.08.007

15. Tran, H.V., Charleux, F., Rachik, M., Ehrlacher, A., Ho-Ba-Tho, M.C.: In vivo characterization of the mechanical properties of human skin derived from MRI and indentation techniques. Comput. Methods Biomech. Biomed. Eng. **10**, 401–407 (2007). https://doi.org/10.1080/10255840701550287

16. Portnoy, S., Yizhar, Z., Shabshin, N., Itzchak, Y., Kristal, A., Dotan-Marom, Y., Siev-Ner, I., Gefen, A.: Internal mechanical conditions in the soft tissues of a residual limb of a trans-tibial amputee. J. Biomech. **41**, 1897–1909 (2008). https://doi.org/10.1016/j.jbiomech.2008.03.035

17. Portnoy, S., Yarnitzky, G., Yizhar, Z., Kristal, A., Oppenheim, U., Siev-Ner, I., Gefen, A.: Real-time patient-specific finite element analysis of internal stresses in the soft tissues of a residual limb: a new tool for prosthetic fitting. Ann. Biomed. Eng. **35**, 120–135 (2007). https://doi.org/10.1007/s10439-006-9208-3

18. Zhang, M., Lord, M., Turner-Smith, A.R., Roberts, V.C.: Development of a non-linear finite element modelling of the below-knee prosthetic socket interface. Med. Eng. Phys. **17**, 559–566 (1995). https://doi.org/10.1016/1350-4533(95)00002-5

19. Holzapfel, G.A.: Nonlinear Solid Mechanics: A Continuum Approach for Engineering Science. Willey, Hoboken (2000)

20. Flynn, C., Taberner, A., Nielsen, P.: Modeling the mechanical response of in vivo human skin under a rich set of deformations. Ann. Biomed. Eng. **39**, 1935–1946 (2011). https://doi.org/10.1007/s10439-011-0292-7

21. Sengeh, D.M., Moerman, K.M., Petron, A., Herr, H.: Multi-material 3-D viscoelastic model of a transtibial residuum from in-vivo indentation and MRI data. J. Mech. Behav. Biomed. Mater. **59**, 379–392 (2016). https://doi.org/10.1016/j.jmbbm.2016.02.020

22. Evans, S.L., Holt, C.A.: Measuring the mechanical properties of human skin in vivo using digital image correlation and finite element modelling. J. Strain Anal. Eng. Des. **44**, 337–345 (2009). https://doi.org/10.1243/03093247JSA488

23. Flynn, C., Taberner, A., Nielsen, P.: Mechanical characterisation of in vivo human skin using a 3D force-sensitive micro-robot and finite element analysis. Biomech. Model. Mechanobiol. **10**, 27–38 (2011). https://doi.org/10.1007/s10237-010-0216-8

24. Salomonsson, K., Zhao, X., Kallin, S.: Analysis of the internal mechanical conditions in the lower limb due to external loads. Int. J. Med. Health Biomed. Bioeng. Pharm. Eng. **10**, 294–300 (2016). https://doi.org/10.5281/zenodo.1124887

25. Shergold, O.A., Fleck, N.A.: Mechanisms of deep penetration of soft solids, with application to the injection. Proc. R. Soc. Lond. Ser. A: Math. Phys. Eng. Sci. **460**, 3037–3058 (2004)

26. Isvilanonda, V., Iaquinto, J.M., Pai, S., Mackenzie-Helnwein, P., Ledoux, W.R.: Hyperelastic compressive mechanical properties of the subcalcaneal soft tissue: An inverse finite element analysis. J. Biomech. **49**, 1186–1191 (2016). https://doi.org/10.1016/j.jbiomech.2016.03.003

27. Bosboom, E.M.H., Hesselink, M.K.C., Oomens, C.W.J., Bouten, C.V.C., Drost, M.R., Baaijens, F.P.T.: Passive transverse mechanical properties of skeletal muscle under in vivo compression. J. Biomech. **34**, 1365–1368 (2001). https://doi.org/10.1016/S0021-9290(01)00083-5

28. Traa, W.A., van Turnhout, M.C., Moerman, K.M., Nelissen, J.L., Nederveen, A.J., Strijkers, G.J., Bader, D.L., Oomens, C.W.J.: MRI based 3D finite element modelling to investigate deep tissue injury. Comput. Methods Biomech. Biomed. Eng. **21**, 760–769 (2018). https://doi.org/10.1080/10255842.2018.1517868

29. Loerakker, S.S., Stekelenburg, A., Strijkers, G.J., Rijpkema, J.J.M., Baaijens, F.P.T., Bader, D.L., Nicolay, K., Oomens, C.W.J.: Temporal effects of mechanical loading on deformation-induced damage in skeletal muscle tissue. Ann. Biomed. Eng. **38**, 2577–2587 (2010). https://doi.org/10.1007/s10439-010-0002-x

30. Chokhandre, S., Halloran, J.P., Van Den Bogert, A.J., Erdemir, A.: A three-dimensional inverse finite element analysis of the heel pad. J. Biomech. Eng. **134**, 1–9 (2012). https://doi.org/10.1115/1.4005692

31. Khaled, E., Khaled, R., Zahouani, H.: Comparison of elastic and tactile behavior of human skin and elastomeric materials through tribological tests khaled. InterSci. Polym. Eng. Sci. (2006). https://doi.org/10.1002/pen

32. Delalleau, A., Josse, G., Lagarde, J.M., Zahouani, H., Bergheau, J.M.: Characterization of the mechanical properties of skin by inverse analysis combined with the indentation test. J. Biomech. **39**, 1603–1610 (2006). https://doi.org/10.1016/j.jbiomech.2005.05.001

33. Silver, F.H., Freeman, J.W., Devore, D.: Viscoelastic properties of human skin and processed dermis. Ski. Res. Technol. **7**, 18–23 (2001). https://doi.org/10.1034/j.1600-0846.2001.007001018.x

34. Delalleau, A., Josse, G., Lagarde, J.M., Zahouani, H., Bergheau, J.M.: A nonlinear elastic behavior to identify the mechanical parameters of human skin in vivo. Ski. Res. Technol. **14**, 152–164 (2008). https://doi.org/10.1111/j.1600-0846.2007.00269.x

35. Alkhouli, N., Mansfield, J., Green, E., Bel, J., Knight, B., Liversedge, N., Tham, J.C., Welbourn, R., Shore, A.C., Kos, K., Winlove, C.P.: The mechanical properties of human adipose tissues and their relationships to the structure and composition of the extracellular matrix. Am. J. Physiol. Endocrinol. Metab. **305**, 1427–1435 (2013). https://doi.org/10.1152/ajpendo.00111.2013

36. Portnoy, S., van Haare, J., Geers, R.P.J., Kristal, A., Siev-Ner, I., Seelen, H.A.M., Oomens, C.W.J., Gefen, A.: Real-time subject-specific analyses of dynamic internal tissue loads in the residual limb of transtibial amputees. Med. Eng. Phys. **32**, 312–323 (2010). https://doi.org/10.1016/j.medengphy.2009.12.006

37. Jia, X., Zhang, M., Lee, W.C.C.: Load transfer mechanics between trans-tibial prosthetic socket and residual limb - Dynamic effects. J. Biomech. **37**, 1371–1377 (2004). https://doi.org/10.1016/j.jbiomech.2003.12.024

38. Lee, W.C.C., Zhang, M., Jia, X., Cheung, J.T.M.: Finite element modeling of the contact interface between transtibial residual limb and prosthetic socket. Med. Eng. Phys. **26**, 655–662 (2004). https://doi.org/10.1016/j.medengphy.2004.04.010

39. Lee, W.C., Zhang, M., Mak, A.F.: Regional differences in pain threshold and tolerance of the transtibial residual limb: Including the effects of age and interface material. Arch. Phys. Med. Rehabil. **86**, 641–649 (2005). https://doi.org/10.1016/j.apmr.2004.08.005

40. Nayak, C., Singh, A., Chaudhary, H.: Topology optimisation of transtibial prosthesis socket using finite element analysis. Int. J. Biomed. Eng. Technol. **24**, 323–337 (2017). https://doi.org/10.1504/IJBET.2017.085438

41. Ramírez, J.F., Vélez, J.A.: Incidence of the boundary condition between bone and soft tissue in a finite element model of a transfemoral amputee. Prosthet. Orthot. Int. **36**, 405–414 (2012). https://doi.org/10.1177/0309364612436409

42. Faustini, M.C., Neptune, R.R., Crawford, R.H.: The quasi-static response of compliant prosthetic sockets for transtibial amputees using finite element methods. Med. Eng. Phys. **28**, 114–121 (2006). https://doi.org/10.1016/j.medengphy.2005.04.019

43. Narracott, A.J., John, G.W., Morris, R.J., Woodcock, J.P., Hose, D.R., Lawford, P.: V: Vessel collapse during external cuff inflation. IEEE Trans. Biomed. Eng. **56**, 273–280 (2009)

44. Zachariah, S.G., Sanders, J.E.: Finite element estimates of interface stress in the trans-tibial prosthesis using gap elements are different from those using automated contact. J. Biomech. **33**, 895–899 (2000). https://doi.org/10.1016/S0021-9290(00)00022-1

45. Cagle, J.C., Reinhall, P.G., Allyn, K.J., McLean, J., Hinrichs, P., Hafner, B.J., Sanders, J.E.: A finite element model to assess transtibial prosthetic sockets with elastomeric liners. Med. Biol. Eng. Comput. **56**, 1227–1240 (2018). https://doi.org/10.1007/s11517-017-1758-z

46. Portnoy, S., Siev-Ner, I., Yizhar, Z., Kristal, A., Shabshin, N., Gefen, A.: Surgical and morphological factors that affect internal mechanical loads in soft tissues of the transtibial residuum. Ann. Biomed. Eng. **37**, 2583–2605 (2009). https://doi.org/10.1007/s10439-009-9801-3

47. Iivarinen, J.T., Korhonen, R.K., Julkunen, P., Jurvelin, J.S.: Experimental and computational analysis of soft tissue stiffness in forearm using a manual indentation device. Med. Eng. Phys. **33**, 1245–1253 (2011). https://doi.org/10.1016/j.medengphy.2011.05.015

48. Iivarinen, J.T., Korhonen, R.K., Jurvelin, J.S.: Experimental and numerical analysis of soft tissue stiffness measurement using manual indentation device—significance of indentation geometry and soft tissue thickness. Ski. Res. Technol. **20**, 347–354 (2014). https://doi.org/10.1111/srt.12125

49. Jijun, S., Haitian, Z., Tongtong, G.: The study of mechanical properties on soft tissue of human forearm in vivo. Int. Conf. Bioinf. Biomed. Eng. (2009). https://doi.org/10.1109/ICBBE.2009.5163671

50. Manafi-Khanian, B., Arendt-Nielsen, L., Graven-Nielsen, T.: An MRI-based leg model used to simulate biomechanical phenomena during cuff algometry: a finite element study. Med. Biol. Eng. Comput. **54**, 315–324 (2016). https://doi.org/10.1007/s11517-015-1291-x

51. Affagard, J.S., Bensamoun, S.F., Feissel, P.: Development of an inverse approach for the characterization of in vivo mechanical properties of the lower limb muscles. J. Biomech. Eng. **136**, 1–8 (2014). https://doi.org/10.1115/1.4028490

52. Then, C., Vogl, T.J., Silber, G.: Method for characterizing viscoelasticity of human gluteal tissue. J. Biomech. **45**, 1252–1258 (2012). https://doi.org/10.1016/j.jbiomech.2012.01.037

53. Dubuis, L., Avril, S., Debayle, J., Badel, P.: Identification of the material parameters of soft tissues in the compressed leg. Comput. Methods Biomech. Biomed. Eng. **15**, 3–11 (2012). https://doi.org/10.1080/10255842.2011.560666

54. Frauziols, F., Chassagne, F., Badel, P., Navarro, L., Molimard, J., Curt, N., Avril, S.: In vivo identification of the passive mechanical properties of deep soft tissues in the human leg. Strain **52**, 400–411 (2016). https://doi.org/10.1111/str.12204

55. Tuan, L.V., Yamamoto, S., Hanafusa, A.: Finite element analysis for quantitative evaluation of a transfemoral prosthesis socket for standing posture. Int. J. Comput. Appl. **170**, 1–8 (2017). https://doi.org/10.5120/ijca2017914658

56. Hendriks, F.M., Brokken, D., van Eemeren, J.T.W.M., Oomens, C.W.J., Baaijens, F.P.T., Horsten, J.B.A.M.: A numerical-experimental method to characterize the non-linear mechanical behavior of human skin. Ski. Res. Technol. **9**, 274–283 (2003). https://doi.org/10.1034/j.1600-0846.2003.00019.x

57. Vannah, W.M., Childress, D.S.: Indentor tests and finite element modeling of bulk muscular tissue in vivo. J. Rehabil. Res. Dev. **33**, 239–252 (1996)

58. Yoshitake, Y., Takai, Y., Kanehisa, H., Shinohara, M.: Muscle shear modulus measured with ultrasound shear-wave elastography across a wide range of contraction intensity. Muscle Nerve **50**, 103–113 (2014). https://doi.org/10.1002/mus.24104

59. Akagi, R., Fukui, T., Kubota, M., Nakamura, M., Ema, R.: Muscle shear moduli changes and frequency of alternate muscle activity of plantar flexor synergists induced by prolonged low-level contraction. Front. Physiol. (2017). https://doi.org/10.3389/fphys.2017.00708

60. Siracusa, J., Charlot, K., Malgoyre, A., Conort, S., Tardo-Dino, P.-E., Bourrilhon, C., Garcia-Vicencio, S.: Resting muscle shear modulus measured with ultrasound shear-wave elastography as an alternative tool to assess muscle fatigue in humans. Front. Physiol. **10**, 1–12 (2019). https://doi.org/10.3389/fphys.2019.00626

61. Nordez, A., Hug, F.: Muscle shear elastic modulus measured using supersonic shear imaging is highly related to muscle activity level. J. Appl. Physiol. **108**, 1389–1394 (2010). https://doi.org/10.1152/japplphysiol.01323.2009

62. Chakouch, M.K., Charleux, F., Bensamoun, S.F.: Quantifying the elastic property of nine thigh muscles using magnetic resonance elastography. PLoS ONE **10**, 1–13 (2015). https://doi.org/10.1371/journal.pone.0138873

63. Diridollou, S., Vabre, V., Berson, M., Vaillant, L., Black, D., Lagarde, J.M., Grégoire, J.M., Gall, Y., Patat, F.: Skin ageing: changes of physical properties of human skin in vivo. Int. J. Cosmet. Sci. **23**, 353–362 (2001). https://doi.org/10.1046/j.0412-5463.2001.00105.x

64. Sanders, R.: Torsional elasticity of human skin in vivo. Pflügers Arch. Eur. J. Physiol. **342**, 255–260 (1973). https://doi.org/10.1007/BF00591373

65. Agache, P.G., Monneur, C., Leveque, J.L., De Rigal, J.: Original contributions mechanical properties and Young's modulus of human skin in vivo. Arch. Dermatol. Res. **269**, 221–232 (1980)

66. Escoffier, C., De Rigal, J., Rochefort, A., Vassalet, R., Lèvêque, J.-L., Agache, P.G.: Age-related mechanical an in vivo study. J. Invest. Dermatol. **93**, 353–357 (1989). https://doi.org/10.1016/0022-202X(89)90058-4

67. Zheng, Y., Mak, A.F.T.: Effective elastic properties for lower limb soft tissues from manual indentation experiment. IEEE Trans. Rehabil. Eng. **7**, 257–267 (1999). https://doi.org/10.1109/86.788463

68. Braus, H., Curt, E.: Anatomie des Menschen. Ein Lehrbuch für Studierende und Ärzte. Springer, Berlin (1940)

69. Snijder, M.B., Dekker, J.M., Visser, M., Bouter, L.M., Stehouwer, C.D.A., Kostense, P.J., Yudkin, J.S., Heine, R.J., Nijpels, G., Seidell, J.C.: Associations of hip and thigh circumferences independent of waist circumference with the incidence of type 2 diabetes: the hoorn study. Am. J. Clin. Nutr. **77**, 1192–1197 (2003). https://doi.org/10.1093/ajcn/77.5.1192

70. Heitmann, B.L., Frederiksen, P.: Thigh circumference and risk of heart disease and premature death: prospective cohort study. BMJ **339**, 736 (2009). https://doi.org/10.1136/bmj.b3292

71. Kuk, J.L., Janiszewski, P.M., Ross, R.: Body mass index and hip and thigh circumferences are negatively associated with visceral adipose tissue after control for waist circumference. Am. J. Clin. Nutr. **85**, 1540–1544 (2007). https://doi.org/10.1093/ajcn/85.6.1540

72. Jung, K.J., Kimm, H., Yun, J.E., Jee, S.H.: Thigh circumference and diabetes: Obesity as a potential effect modifier. J. Epidemiol. **23**, 329–336 (2013). https://doi.org/10.2188/jea.JE20120174

73. Liao, P.J., Lin, T.Y., Ting, M.K., Peng, T.I., Chiou, W.K., Chen, L.H., Hsu, K.H.: Chest width, waist circumference, and thigh circumference are predictors of dementia. Int. J. Geriatr. Psychiatry **33**, 1019–1027 (2018). https://doi.org/10.1002/gps.4887

74. Giorgio, I., dell'Isola, F., Steigmann, D.J.: Axisymmetric deformations of a 2nd grade elastic cylinder. Mech. Res. Commun. **94**, 45–48 (2018). https://doi.org/10.1016/j.mechrescom.2018.09.004

75. Ben-Or Frank, M., Niestrawska, J.A., Holzapfel, G.A., deBotton, G.: Micromechanically-motivated analysis of fibrous tissue. J. Mech. Behav. Biomed. Mater. **96**, 69–78 (2019). https://doi.org/10.1016/j.jmbbm.2019.04.007

76. Puertolas, S., Pena, E., Herrera, A., Ibarz, E., Gracia, L.: A comparative study of hyperelastic constitutive models for colonic tissue fitted to multiaxial experimental testing. J. Mech. Behav. Biomed. Mater. **102**, 103507 (2020). https://doi.org/10.1016/j.jmbbm.2019.103507